



## WIND-DRIVEN DAMAGE LOCALIZATION ON A SUSPENSION BRIDGE

Marco Domaneschi<sup>1</sup>✉, Maria Pina Limongelli<sup>2</sup>, Luca Martinelli<sup>3</sup>

<sup>1, 3</sup>Dept of Civil and Environmental Engineering, Technical University of Milan,  
Piazza Leonardo da Vinci 32, 20133 Milan, Italy

<sup>2</sup>Dept of Architecture, Built Environment and Construction Engineering, Technical University of Milan,  
Piazza Leonardo da Vinci 32, 20133 Milan, Italy

E-mails: <sup>1</sup>marco.domaneschi@polimi.it; <sup>2</sup>mariapina.limongelli@polimi.it; <sup>3</sup>luca.martinelli@polimi.it

**Abstract.** The paper focuses on extending a recently proposed damage localization method, previously devised for structures subjected to a known input, to ambient vibrations induced by an unknown wind excitation. Wind induced vibrations in long-span bridges can be recorded without closing the infrastructure to traffic, providing useful data for health monitoring purposes. One major problem in damage identification of large civil structures is the scarce data recorded on damaged real structures. A detailed finite element model, able to correctly and reliably reproduce the real structure behavior under ambient excitation can be an invaluable tool, enabling the simulation of several different damage scenarios to test the performance of any monitoring system. In this work a calibrated finite element model of an existing long-span suspension bridge is used to simulate the structural response to wind actions. Several damage scenarios are simulated with different location and severity of damage to check the sensitivity of the adopted identification method. The sensitivity to the length and noise disturbances of recorded data are also investigated.

**Keywords:** damage localization, finite element, long-span bridge, monitoring, noise, wind.

### 1. Introduction

Current trends for monitoring large civil structures include the use of permanent networks of sensors, enabling the continuous in-service monitoring of the health conditions of the structure. These networks allow to automatically record the structural responses that, if used together with an efficient and reliable method of damage identification, allow to constantly monitor the health of strategic structures and infrastructures. A major benefit of such monitoring systems, beside the possibility of a fast detection and a prompt intervention in case of damage, is the possibility to move from a scheduled-based maintenance program to a condition-based maintenance, carried out “on request” on the base of the effective health state of the structure. In literature (Doebeling *et al.* 1998) several methods for vibration-based damage identification have been proposed at several levels of refinement; from level I to IV, these are: damage detection, localization, quantification, and prediction of the remaining service life. Response to forced vibrations can be used for damage identification purposes but may be scarcely effective for large and flexible structures such as suspension bridges, with modal frequencies within the frequency range 0–1 Hz. On the contrary the analysis of the response to ambient vibrations can provide

useful information despite the relatively low amplitude of the responses (Abdel-Ghaffar, Scanlan 1985; Brownjohn *et al.* 1987; Catbas, Aktan 1999). Wind loading is one of the environmental excitations inducing vibrations that can be recorded on bridges for very long periods without interrupting the operating conditions of the infrastructure (He *et al.* 2008; Cunha 2013 *et al.*), allowing both a better resolution in the frequency domain and a reduction of the effect of noise by the averaging of data.

The focus of this paper is the extension to the case of ambient vibrations due to an unknown input of a recently proposed damage localization method previously applied to structures subjected to vibrations induced by a known input. The selected damage localization algorithm, known as Interpolation Damage Detection Method (IDDM), is based on a damage feature defined in terms of the error related to the interpolation of the structure’s operational deformed shapes with a spline function. Specifically the variation of the interpolation error between two configurations of the structure highlights the existence of damage at a location close to the one where the variation of the interpolation error is detected. In the previous applications of the IDDM ordinary (medium to small size) and large structures were considered subjected to a base seismic

excitation, or to an impulse (Dilena *et al.* 2014; Domaneschi *et al.* 2012, 2013a, 2013b; Limongelli 2010, 2011, 2014), assuming the input could be measured. In order to perform this task, responses to vibrations of the structure in the original (undamaged) and in a damaged configuration are needed. In a real application of the method such responses would be directly measured on the monitored structure. For the assessment and calibration of the damage identification algorithms one major issue is the scarce availability of data recorded on real damaged structures. Indeed, even if there are several data on seriously damaged structures, information on well instrumented structures is lacking. This is the main reason why analytical methods proposed in literature are almost invariably tested on scaled-down laboratory specimens (Yonggang *et al.* 2008; Zhou *et al.* 2007) or using numerical simulations. The availability of a detailed finite element model, able to correctly and reliably reproduce both the real behavior of the structure under ambient excitations and also the ambient excitation is an invaluable tool for the simulation of several different damage scenarios aimed at testing the performance of monitoring systems.

In this paper, a calibrated three dimensional finite element (FE) model of a long-span existing suspension bridge, the Shimotsui-Seto bridge, has been used to simulate the structural response to wind excitation. The numerical model has been built and validated through original design tables and measures (modal frequencies and shapes). Such data have been provided thanks to the HSBE Authority which manages the bridge. The availability of such a detailed and calibrated model has allowed to pursue the extension of the IDDM to the case of ambient vibrations, considering the sensitivity of IDDM to damage location, to noise in the recorded signals, to length of the recorded responses, as well as the mutual influence of noise and signal duration. The effect of geometric nonlinearities on the sensitivity of the IDDM was also investigated. This aspect is particularly important for the case of flexible structures such as suspension bridges, since for this type of structures the effect of the geometric nonlinearity is not negligible and the damage identification algorithm is based on the structure's operational deformed shapes that can indeed be influenced.

Wind acting in the horizontal direction, transversally to the deck, is assumed as the source of ambient excitation. It is reproduced as a spatially correlated process and only drag forces are considered (Domaneschi *et al.* 2013c). Analyses are carried out to characterize the “signature” of the pristine and damaged structure, adopting a mean wind velocity of 10 m/s which corresponds to a “Fresh Breeze” in the Beaufort wind scale. This is to assure a very small return period for similar low-intensity wind velocities, and hence to collect a large set of data to perform damage detection analyses.

Several damage scenarios have been simulated by changing the bending stiffness of the of the bridge deck elements. Furthermore, following an approach widely employed in literature (Nguyen, Tran 2010; Zhu, Law 2006) responses from the numerical model have been corrupted with a white Gaussian noise, considering different values of the Gaussian process variance. Finally, different lengths of the simulated responses have been considered to research the reciprocal influence between noise and signal duration.

## 2. The Shimotsui-Seto bridge and its numerical model

The suspension bridge considered here as a case study is located in Japan: the Shimotsui-Seto bridge (Fig. 1a) is spanning from the side of Mt. Washu to Hitsuishijima Island. The main geometric dimensions of the structure are: length 1400 m; length of main span 940 m; height of the towers 149 m; elevation of the main girder above the foundation of the towers 31 m; width and thickness, respectively, of main girder cross-section 30×13 m. The steel frame deck is of a stiffened truss type. The towers, the hangers and the main cables are steel elements.

In transient dynamic analyses of long span flexible bridges the geometric nonlinearities play a significant role in the system response. This it is evident by comparing the frequencies of the natural vibration modes evaluated on the unstressed structure with those evaluated on the stressed structure (e.g. under its self-weight). In the last condition the structural model results generally stiffer and, consequently, is characterized by higher natural frequencies. Thus, the FE analyses on the bridge model have been carried out taking into account the geometric nonlinearities that characterize such problems. The natural modal shapes have been calculated by



**Fig. 1.** The structure and FE models : a – Shimotsui-Seto suspension bridge (by Tatushin, September 2008; with permission); b – detailed bridge model for matching the real modal characteristics; c – validated simplified bridge model used in the analyses

considering the stressed condition of the bridge caused by its self-weight. The dynamic equilibrium in transient analyses of the bridge structural model has been evaluated in the deformed shape due to inertial forces, the dead loads (weight of the structural elements) and the dynamic forces coming from interaction with the wind.

The configuration at rest for the bridge has been computed accounting for the structure self-weight with the iterative correction of the nodes position as it follows. An initial stressed configuration was found by applying the self-weight of the structural elements. This configuration is not the one specified by design, and the displacement field needs correction. This consisted in the uplifting of the girder nodes through the shortening of the suspenders, and allows for reaching the design configuration of the bridge including also some tension stiffening. The FE model, calibrated by the described multi-step procedure, achieves a satisfactory approximation of the real structure dynamic behavior, as arises from matching the modal parameters as discussed in the remaining of this section.

The suspension bridge was numerically modeled within the ANSYS framework at two different levels of refinement. A first model (Fig. 1b), more detailed, implements an almost one-to-one correspondence between FE elements and structural members. Its properties (geometrical and mechanical) have been assessed by the match of the first four modal shapes and natural periods with the ones determined on the real structure (Table 1). The natural periods, and corresponding mode shapes for the first four modes have been provided by the bridge Authority and came from on-site surveys using the existent sensors network on the bridge structure. The purpose of this model (Fig. 1b) was to aid in the development of a second, simpler, model (Fig. 1c) to be used to ease the computationally expensive nonlinear transient analyses under wind loading. Such simplified model adopts for the deck girders an equivalent beam

model based on Timoshenko’s beam kinematics. The beam is located at the main girder cross-section centroid and is connected to the cable system by rigid members to reproduce the geometry of the suspension system.

The accuracy of the simplified model (Fig. 1c) was assessed: (i) by comparing its first four modal frequencies and shapes against the experimental values and against the values derived from the detailed bridge model (Fig. 1b); (ii) by comparing the parameters of its higher modes against the values derived from the detailed bridge model, since no experimental data were available for these modes. The equivalence of the simplified version of the bridge model with the detailed one was proven through the well known Modal Assurance Criterion (Allemang, Brown 1982; MAC): a value of MAC close to 0 means inconsistency between the compared modal shapes while a MAC index close to 1 indicates a good consistency. The values of the MAC index reported in Table 2 show that the two structural models can be considered equivalent both in terms of the natural frequencies and of modal shapes. The interested reader is pointed to (Domaneschi, Martinelli 2013) for further details on the numerical models.

### 3. Wind loading on the FE model

At each time step  $t_n$  of the transient dynamic analyses the wind loading is computed from knowledge of the turbulent wind velocity. The stationary random field of spatially variable turbulent wind velocity is computed at the (initial) position of the nodes of the FE model as:

$$\mathbf{v}(\mathbf{M}_k, t_n) = \mathbf{v}_m(\mathbf{M}_k) + \mathbf{v}'(\mathbf{M}_k, t_n), \quad (1)$$

where  $\mathbf{M}_k$  – the vector defining the (initial) position of node  $k$ ;  $t_n$  – the  $n$ -th time step;  $\mathbf{v}_m$  – the mean wind velocity vector;  $\mathbf{v}'$  – the vectorial zero mean turbulent fluctuation

**Table 1.** Modal frequencies for the real structure (Courtesy of Mr. M. Nishitani HBSE-JP) and the bridge models

Mode	Real structure, Hz	Detailed model, Hz	Simplified model, Hz	Modal shape
1	0.10	0.10	0.10	Lateral symmetric
2	0.16	0.15	0.15	Vertical anti-symmetric
3	0.20	0.23	0.23	Vertical symmetric
4	0.25	0.25	0.26	Lateral anti-symmetric

**Table 2.** Modal frequencies of the simplified bridge model and MAC coefficients.

Mode	Modal shape	MAC	Frequency, Hz	Mode	Modal shape	MAC	Frequency, Hz
L1	Lateral symmetric	0.99	0.10	V1	Vertical anti-symmetric	1.00	0.15
L2	Lateral anti-symmetric	0.99	0.26	V2	Vertical symmetric	0.99	0.23
L3	Lateral symmetric	0.98	0.45	V3	Vertical anti-symmetric	0.99	0.47
L4	Lateral anti-symmetric	0.78	0.68	V4	Vertical symmetric	0.99	0.71
L5	Lateral symmetric	0.95	0.94	V5	Vertical anti-symmetric	0.99	0.97
T1	Torsional symmetric	0.97	0.52	V6	Vertical symmetric	0.99	1.28
T2	Torsional anti-symmetric	0.97	0.80				
T3	Torsional symmetric	0.92	1.22				

of  $\mathbf{v}$  around  $\mathbf{v}_m$ . With reference to the unit vectors  $\bar{i}$ ,  $\bar{j}$ ,  $\bar{k}$  along the longitudinal, transversal and vertical direction, respectively, of the bridge, the turbulent velocity  $\mathbf{v}'$  is represented by its components as:

$$\mathbf{v}'(\mathbf{M}_k, t_n) = \bar{i}u'(\mathbf{M}_k, t_n) + \bar{j}l'(\mathbf{M}_k, t_n) + \bar{k}w'(\mathbf{M}_k, t_n). \quad (2)$$

For the aim of this damage detection study the wind velocity is spatially correlated and is described by its power spectral density and a coherency model, while the turbulence components  $u'$  and  $w'$  are assumed as zero. The

$$P(\omega) = \begin{bmatrix} P(\omega) & \gamma_{12}(\omega)\sqrt{P_1(\omega)P_2(\omega)} & \dots & \gamma_{1n}(\omega)\sqrt{P_1(\omega)P_n(\omega)} \\ \gamma_{21}(\omega)\sqrt{P_2(\omega)P_1(\omega)} & P_2(\omega) & \dots & \gamma_{2n}(\omega)\sqrt{P_2(\omega)P_n(\omega)} \\ \dots & \dots & \dots & \dots \\ \gamma_{n1}(\omega)\sqrt{P_n(\omega)P_1(\omega)} & \gamma_{n2}(\omega)\sqrt{P_n(\omega)P_2(\omega)} & \dots & P_n(\omega) \end{bmatrix}, \quad (3)$$

$$v'_i = \sum_{m=1}^i \sum_{n=1}^N A_{im}(\omega_n) \cos[(\omega_n t) + \beta_{im}(\omega_n) + \varphi_{mn}]. \quad (4)$$

The coherency function relates different components at the same points (“point” coherency) or equal components at different points in space (“space” coherency). The decay of the space coherency with the distance between nodes  $i$  and  $j$  is of the exponential type. The coherency function model is entirely defined when the terrain factor, the minimum height, the roughness length and the average velocity are known. These come from *EN 1991-1-4:2005 Eurocode 1 Actions on Structures – General Actions – Wind Actions* for a classification of the site of the bridge as sea or coastal area (terrain category 0). The turbulent wind velocity records are generated at the required nodal positions  $\mathbf{M}_k$  following the conditional simulation procedure by Hao *et al.* (1989). The velocity time history  $v'_i = \bar{j}l'$  at node  $i$  is obtained from the finite series (Eq (4)).

In the numerical simulations the circular frequencies  $\omega_n$  are assumed to vary in the interval  $-\omega_N \leq \omega_n \leq \omega_N$ , where  $\omega_N = \frac{2\pi}{2\Delta t}$  is the Nyquist frequency and  $\Delta t$  the time step (here 0.1 s). The terms  $\varphi_{mn}$  are random variables, characterized by a uniform probability density in the range from 0 to  $2\pi$ , that are statistically independent, for  $m \neq r$  and  $n \neq s$ , from  $\varphi_{rs}$ . The phase angles  $\beta_{im}$  and the amplitudes  $A_{im}$  are selected in a way to make Eq (3) satisfied.

The structural model is subjected, given the previous observations, to a turbulent wind field having the mean velocity transversal to the longitudinal bridge axis and horizontal. The ensuing wind loading is applied to the cables, the deck and the towers in the direction transversal to the bridge span. The forces due to the suspenders have been divided into two parts, applied to the main girder (at the bottom) and the main cable (at the top of the suspenders), respectively. The model for the wind interaction forces comprises the contribution of the drag only (Eq (5)), where

turbulent fluctuations of the wind velocity are seen as realizations of a zero mean stationary stochastic process defined by the 3D turbulence model by Solari and Piccardo (2001). This model is based on the definition of direct spectral densities  $P_i(\mathbf{M}_i, \omega)$  and coherency functions  $\gamma_{ij}(\mathbf{M}_i, \mathbf{M}_j, \omega)$ , where  $\omega$  is the circular frequency. The elements of the matrix of the cross spectral densities  $P_{ij}(\mathbf{M}_i, \mathbf{M}_j, \omega)$ , between stations  $i$  and  $j$ , can be written in terms of the coherency functions  $\gamma_{ij}(\mathbf{M}_i, \mathbf{M}_j, \omega)$  and the direct power spectral densities  $P_i(\mathbf{M}_i, \omega)$ ,  $P_j(\mathbf{M}_j, \omega)$  (omitting dependency from  $\mathbf{M}_i$  and  $\mathbf{M}_j$  for brevity) as:

$$F_D(M, t) = \frac{1}{2} \rho_a C_D(\alpha_a) [v(M, t)]^2 A(M). \quad (5)$$

$A(M)$  – the surface area of the element exposed to the wind action;  $\rho_a$  – the air density;  $C_D$  – the drag coefficient;  $\alpha_a$  – the angle of attack. This modeling choice simplifies, on the one hand, the computation of this type of forces while, on the other hand, it has been proved to correlate well with a more advanced description of the wind interaction forces based on an indicial function representation (Domaneschi, Martinelli 2014).

Evaluation of the drag coefficient for the main girder is performed from the available wind tunnel test curve (Courtesy of Mr. M. Nishitani HBSE-JP), relating the angle of attack to the drag coefficient. For the bridge towers, the hangers and the main cables, such characteristics have been taken from literature (Domaneschi, Martinelli 2013). An average velocity of 10 m/s for the wind has been assumed in the dynamic analyses.

#### 4. Procedure for damage detection and localization

The method applied to detect and localize damage on the bridge structural model is the IDDM which reposes on an estimation of the operational deformed shapes of the structure. The method does not necessitate a precise knowledge of the modal shapes, neither in the structure pristine state nor in the one damaged, thus avoiding the bothersome operations connected to the identification and validation of the modal shapes (Casati *et al.* 2005a, 2005b; Ratcliffe 2000; Sampaio *et al.* 1999), furthermore, its simplicity and computational efficiency make it an ideal candidate for automation purposes. The IDDM was originally presented in (Limongelli 2010, 2011) for seismically excited structures and later applied to other types of excitations but always considering the input to be known. In the case of ambient vibrations the input is generally unmeasured hence the original formulation of the IDDM, based on the estimation of the Frequency Response Functions (FRFs) with

respect to the input forcing function, needs to be modified. In the case of a structure excited by a single known input, the magnitude of the FRF at each location  $z$  can be easily estimated using the relationship between the power spectral densities (PSDs) of the input and the output:

$$\mathbf{P}_z = \mathbf{H}_{xz}^{T*}(f) \mathbf{P}_i(f) \mathbf{H}_{xz}(f), \quad (6)$$

where  $f$  – the frequency value;  $\mathbf{P}_z(f)$  – the PSD matrix of the responses;  $\mathbf{P}_i(f)$  – the PSD matrix of the inputs;  $\mathbf{H}_{xz}$  – the FRF matrix for the frequency domain decomposition; the subscript “\*” and superscript “T” denote respectively the complex conjugate and the transpose. If the input can be assumed to be a white noise, hence with a constant power spectral density ( $\mathbf{P}_i(f) = \mathbf{C}$ ), Eq (6) can be written as:

$$\mathbf{P}_z = \mathbf{H}_{xz}^{T*}(f) \mathbf{C} \mathbf{H}_{xz}(f). \quad (7)$$

The assumption of constant PSD of the input, even if not strictly verified, is widely applied in output only system identification. The Natural Excitation Techniques method (James *et al.* 1995), the Frequency Domain Decomposition method (Brickner *et al.* 2000), the Stochastic Subspace Identification methods (Peeter *et al.* 2001) are all examples of techniques based on the assumption of white noise input to simulate the input in case of ambient excitations. In Fig. 2a surface representation of matrix  $\mathbf{P}_z(f)$  is given for the frequency range 0÷0.4 Hz, assuming that responses are recorded at 71 locations along the bridge deck. Each row corresponds to a function  $P(z, f)$ , such functions are reported for the numerical model of the bridge under wind loading that is addresses in Sections 3 and 4. Even if the assumption of constant power spectral density of the input is not strictly verified for the herein case considered, it can be seen that the PSDs describe the profile of the magnitude of the deformed shape at different frequencies. In principle, at a generic frequency the deformed shape derives from the superposition of different modal contributions but near to a modal frequency (at resonance) the profile is clearly dominated by the relevant modal shape. The feature used for damage detection is defined in terms of the error from use of cubic spline functions in modeling the deformed configuration of the bridge deck. More specifically, the modeling accuracy is defined at any given location as

the difference of the displacement measured and the one at that same location calculated by interpolation with a proper function of the measured displacements at all the other locations outfitted with a sensor.

Eq (7) allows to reformulate the definition of the damage feature on which the IDDM is based not on the base of FRFs but in terms of the PSD of the responses. The interpolation error is then defined as a function of the power spectral densities  $\mathbf{P}$  of recorded (R) and interpolated (S) accelerations:

$$E(z, f_i) = P_R(z, f_i) - P_S(z, f_i), \quad (8)$$

where  $P_R$  – the PSD of the response recorded at location  $z$ ;  $P_S$  – the spline interpolation of the PSD at  $z$ . In order to characterize each location with a single error parameter, the norm of the error on the whole range of frequencies is considered:

$$E(z) = \sqrt{\sum_1^N E(z, f_i)^2}, \quad (9)$$

where Eq (9)  $N$  – the number of the PSD frequency lines inside the frequency range in which the signal-to-noise ratio is sufficient to allow for a correct definition of the PSD. The PSD value depends on the structure’s state, therefore, if the error function is estimated with Eq (9) in the baseline (undamaged) and in the inspection (potentially damaged) states, respectively  $E_0$  and  $E_d$ , the comparison between these two values should give an indication about damage existence at the location considered. A stiffness variation associated with damage drives a change in the operational deformed shape pointed out by an increase of the interpolation error going from the reference ( $E_0$ ) to the current configuration ( $E_d$ ). Consequently the damage parameter is defined as follows:

$$\Delta E(z) = E_d(z) - E_0(z), \quad (10)$$

where parameter  $\Delta E$  – affected by some randomness. In order to remove this effect, and assuming a Normal distribution for it, a threshold value of the damage parameter is selected, and the damage index is defined as:

$$D(z) = \Delta E(z) - \Delta E_T. \quad (11)$$

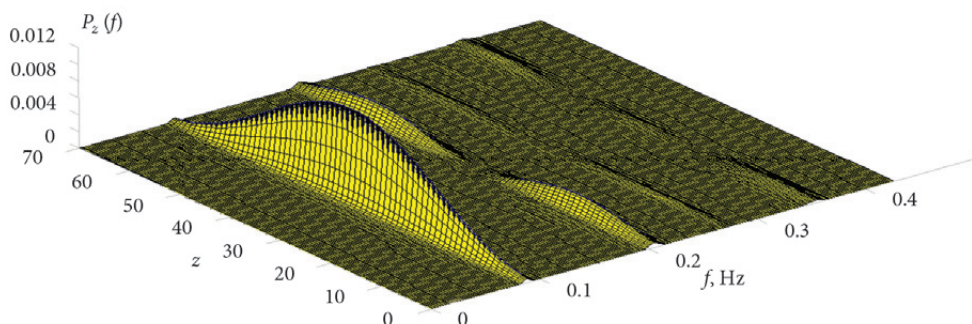


Fig. 2. Power spectral densities of the responses at the measurement points

The threshold value is defined as  $\Delta E_T = \mu_{\Delta E} + \nu\sigma_{\Delta E}$ , being  $\mu_{\Delta E}$  and  $\sigma_{\Delta E}$  the mean and the variance, respectively, of the damage parameter  $\Delta E$  over the set of records available, and  $\nu$  the quantile  $Z_{1-\alpha}$  of the standard normal distribution corresponding to the accepted probability ( $\alpha$ ) of false alarms. In this work a value  $\nu = 2.32$ , which corresponds to a 2% accepted probability of false alarms, has been assumed. Once the threshold is known, the Interpolation Damage Index can be calculated at location  $z$  as the positive difference between the actual value of the interpolation error and the threshold:

$$\begin{aligned} IDI(z) &= \Delta E(z) - \Delta E_T \text{ if } \Delta E(z) \geq \Delta E_T, \\ IDI(z) &= 0 \text{ if } \Delta E(z) < \Delta E_T. \end{aligned} \quad (12)$$

The interpolation error is also affected by several other phenomena, such as noise in recording sensors or environmental variations of temperature and/or humidity or even traffic. All these sources are certainly independent and induce random variations of the interpolation error. Thus, according to the Central Limit Theorem, if the variation of a physical quantity is caused by several small, independent, random sources then the distribution function of this quantity is well approximated by the normal distribution (Soong 2004).

### 5. Instrumentation and damage scenarios on the bridge model

To assess the performance of the IDDM under wind loading, several different damage scenarios were simulated on the numerical model of the bridge. The bridge has been assumed as instrumented at each node of the central span in the FE model with unidirectional accelerometers placed onto the deck. The nodes are numbered from left to right from N1 to N71 (Fig. 3), with node N36 at the deck mid-span. The responses time-histories recovered from transient analyses of the bridge FE model at these locations are assumed as if they were recorded on the bridge. Additionally, to assess the impact of noise on the IDDM, Gaussian white noise of different intensity was added to the responses time-histories.

In order to investigate the sensitivity to the noise level of the damage detection method, three different situations have been considered, corresponding to decreasing levels of the Signal-to-Noise-Ratio (SNR): SNR = 1000 (low noise); SNR = 50 (medium noise); SNR = 20 (high noise). These correspond to a root mean square (RMS) of the

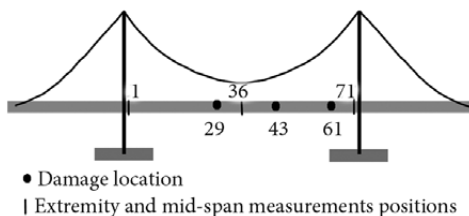


Fig. 3. Location of measurements and damage points

noise of 0.1%, 2% and 5% respectively, of the RMS of the accelerations recorded. Noise depends primarily on the quality of the sensors and, more in general, on the data acquisition hardware and software used, and on the measuring procedure adopted. Several other noise sources can also be important, ranging from electric power fluctuations, to air currents, to stray radiation from nearby electrical equipment and so on. It is quite difficult to predict the many on site possible “pollution” sources as well as the value of the noise level. The decision to use 0.1%, 2% and 5% noise levels was aimed to investigate a wide range of possible real conditions and to evaluate their impact on the performance of the IDDM algorithm. This choice is also in agreement with the existent literature (e.g. Hester, González 2015; Mohd-Yasin et al. 2010). It is worth noting that the selected range of noises corresponds also to the sensors commercial range. In particular, the noise increases as the device costs decreases, with sensors of low noise characteristics in the order of 100 EUR per channel (Domaneschi et al. 2013a).

A stiffness reduction in the beam elements simulates damage at a nodal position along the deck in the elements jointed at nodes 29, 43 and 61 (Fig. 3). Different damage levels have been considered assuming a stiffness percentage reductions of 15–75%. The loss of stiffness is intended to represent a series of potential conditions in the steel frame bridge deck such as loss of section area or failure of connections in braces and main longitudinal beam elements. Damage in the structural elements can be due to several causes, e.g. a preceding extreme event, such as a strong earthquake or a hurricane, or it can be induced by progressive degradation in a long time scenario due to corrosion and fatigue (Hendy, Chakrabarti 2014). The severity of damage is chosen to be in line with damage levels used in the literature. For example in references (Nguyen, Tran 2010; Zhu, Law 2006) the authors modelled damage of increasing severity through stiffness losses in the range of 0% to 85%.

Two different wind loading episodes have been considered to characterize the damage state of the structure: one on the intact and one on the damaged configurations of the bridge. Each episode comprises a realization of a turbulent wind velocity field. The considered loadings represent two realization of the same stochastic process and hence share the same mean wind speed and statistical properties (cross and direct Power Spectral Density functions) while being otherwise unrelated. This choice entails that each wind event with a predefined average wind speed will respect the same cross and direct Power Spectral Density functions.

In order to analyze for in the case of noisy signals the influence of the records length on the sensitivity of the method, for each damage scenario, and level of noise, three different length of the recorded signals have been tested. Namely, record’s lengths of 16.5 min, 330 min and 660 min have been considered. In the following, a selection of results considered representative of the mutual relationship between level of noise and records length is reported.

### 6. Results

Figs 4–9 report for the previously described damage scenarios the results of the IDDM application. In these figures, the sensitivity of the damage parameter to the severity and to the location of damage, to the level of noise in recorded signals and to the duration of the available recorded responses is reported. A large number of damage scenarios was simulated but only a selection of results is reported herein to avoid being repetitive.

Sensitivity with respect to damage severity has been studied at one single location. In this first part of the investigation, the effect of noise was neglected and responses not corrupted by noise were considered for the estimation of the damage parameter. Fig. 4 shows the results obtained for locations N43 and N61, in the case damage is gradually increased from 15% to 60%. The blue bar gives the real position of damage, the different black lines report the values of the damage parameter at all the instrumented locations for different severities of damage. As expected, the values of  $\Delta E$  steadily increases with the level of damage at both locations but the comparison between the two figures shows that the damage parameter has lower values at location N61 with respect to location N43, even if the severity of damage is the same at these two locations. This trend, which is common to all the scenarios with one damaged location along the bridge deck, indicates that the damage parameter  $\Delta E$  increases with the severity of damage but its intensity depends on the particular location of damage. Thus, in the present formulation, though the IDDM is able to localize the damage it exhibits values that are not uniquely correlated to its severity: the same value of the damage parameter may correspond to different damage severities depending on the location. It follows that the IDDM cannot give quantitative information about the severity of damage at a given location. The investigation of this capability, which would move the IDDM to a method of damage identification of Level III (damage quantification), is beyond the scope of this work and will not be pursued further in this work.

The sensitivity to noise of the IDDM has been investigated considering results obtained for several single and multiple damage scenarios based on signals polluted with increasing levels of noise. Some results, relevant to scenarios with both single and multiple damage locations are reported in Figs 5 to 9 where the black line depicts the damage parameter  $\Delta E(z)$ , the blue bar gives the real position of damage and the black dotted line the threshold related to a 2% probability  $\alpha$  of false alarms. This threshold defines the minimum value of  $\Delta E(z)$  denouncing a damage at location  $z$ .

At first an analysis was carried out to show that in the case of inspection of an undamaged structure the method is able to give information about the actual health state of

the structure, results are reported in Fig. 5. Due to noise in recorded signals the damage parameter exhibits values different from zero in several positions but the values are always under threshold corresponding to a 2% accepted probability  $\alpha$  of false alarms, hence are discarded by the damage criterion defined in Eq (12).

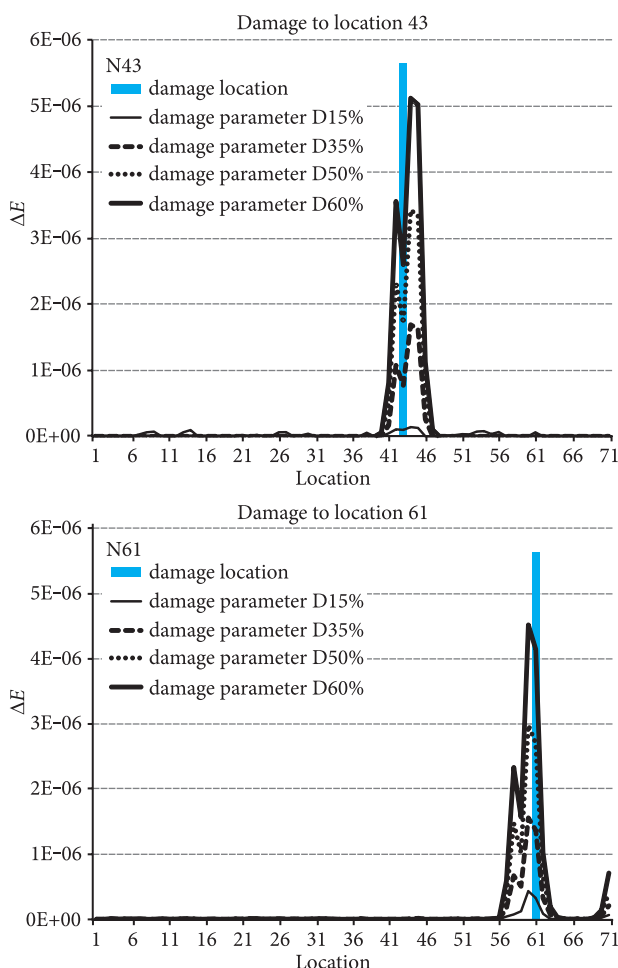


Fig. 4. Sensitivity of the damage parameter to the damage severity

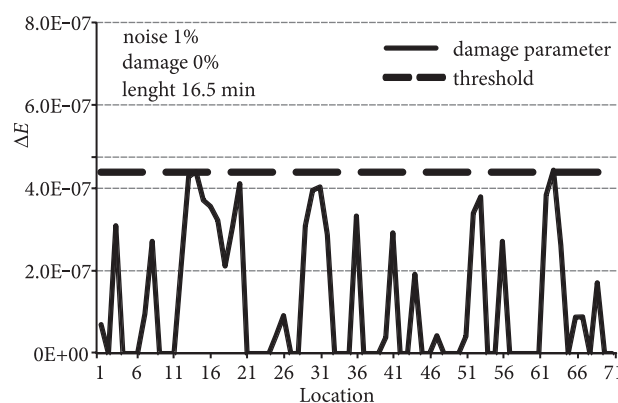


Fig. 5. Damage parameter and threshold for an undamaged configuration: 1% noise and 16.5 min response length

Fig. 6 reports results for a single damage scenario (damage at location N43) and several levels of noise and lengths of the responses. Only results for minimum recording lengths of those allowed for the correct detection of the damaged location are reported. Provided that the length of the recorded signals increases with the noise level, a stiffness reduction of 50% is correctly detected for all noise levels. Smaller damages can be correctly identified if the noise level

is small, but are impossible to detect even for very long signals if the noise level increases over 2%.

Figs 7a to 7d report the results for a scenario of multiple damage (two damaged locations that coexist on the structure) obtained under the assumption of low noise (0.1%), for different severities of damage (from 20% to 75% stiffness reduction). A total length of the recorded responses of 16.5 min has been considered. In this case the positions damaged are

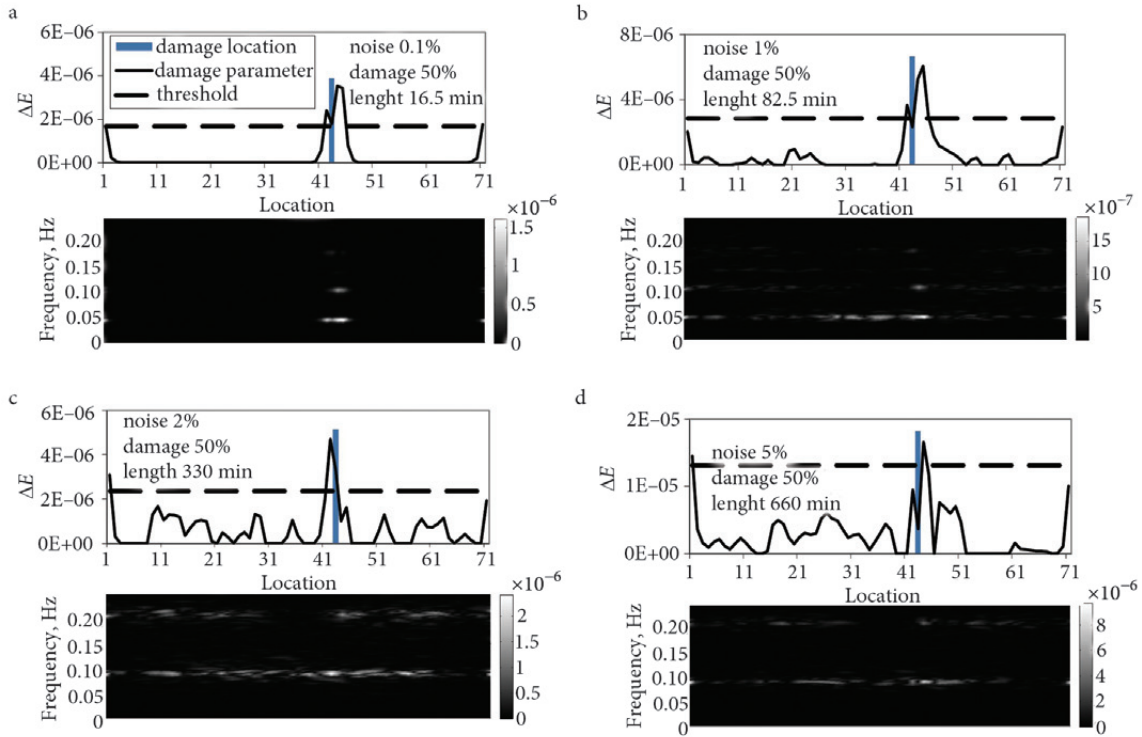


Fig. 6. Single damage for different levels of noise and lengths of the responses. Contour bands:  $|E_d(z) - E_o(z)|$

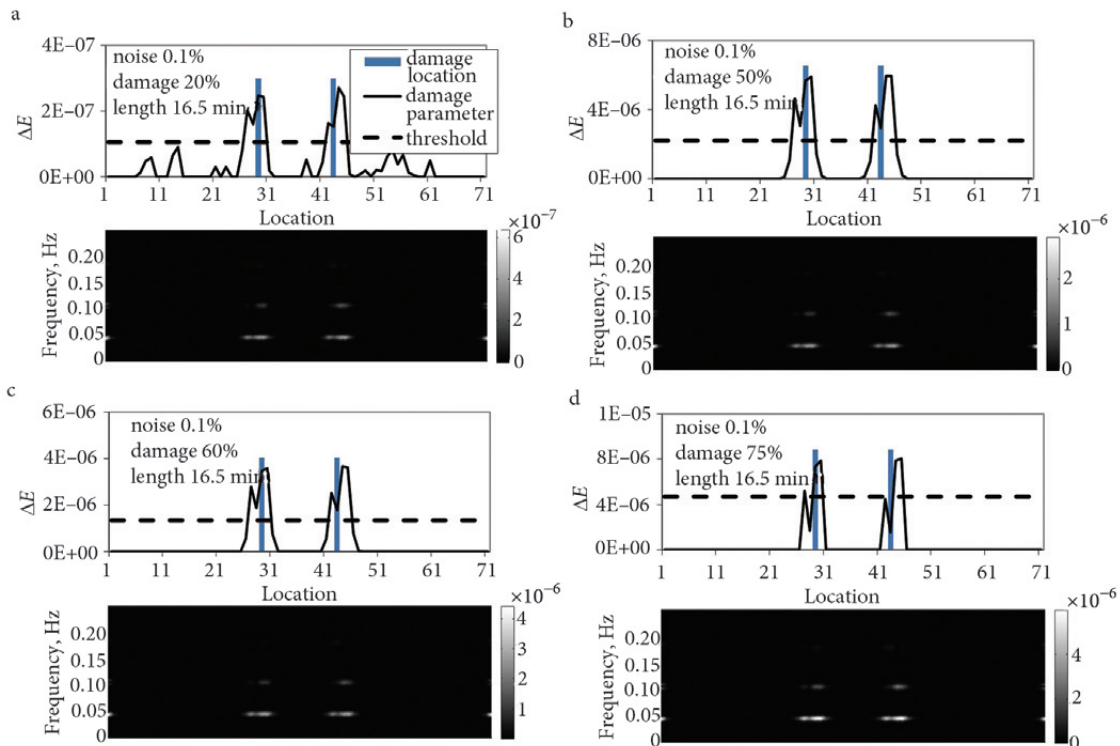


Fig. 7. Multiple damage scenario for response length of 16.5 min and  $\text{SNR} = 1000$ . Contour bands:  $|E_d(z) - E_o(z)|$

clearly detected, most notably also for the smaller value of damage (Fig. 7a). The damage parameter shows values above zero also at non damaged locations, but these values are under the threshold and hence have to be discarded according to the proposed damage localization algorithm.

As the noise level increases (Fig. 8, corresponding to 2% noise) detection outcomes become less reliable. For this figure, results obtained for a longer duration of the recorded

signals (330 min) are reported, because shorter responses did not allow detection even for very high levels of damage. For this noise level severe damages (higher than 60%) are correctly located (Figs 8c, 8d) while several false alarms appear in the case of minor damages (Figs 8a, 8b).

As a general comment, the longer are the records, and the higher is the damage level, the higher appears the sensitivity of the method in detecting the positions damaged

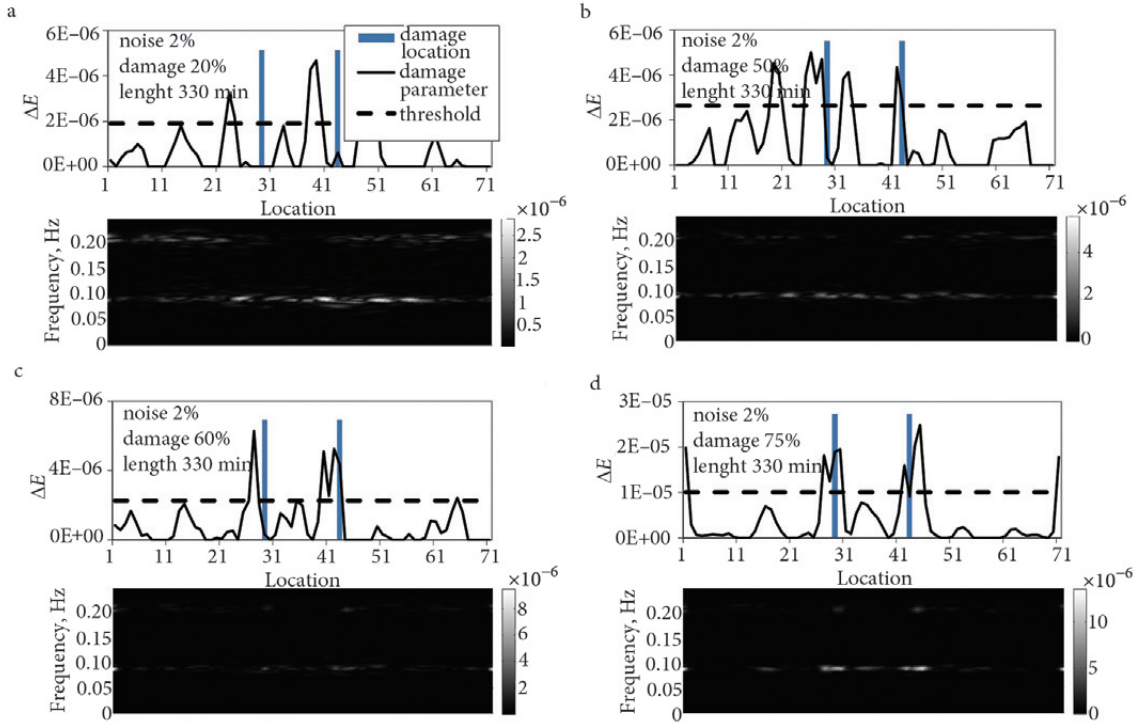


Fig. 8. Multiple damage scenario for response length of 330 min and SNR = 50. Contour bands:  $|E_d(z) - E_o(z)|$

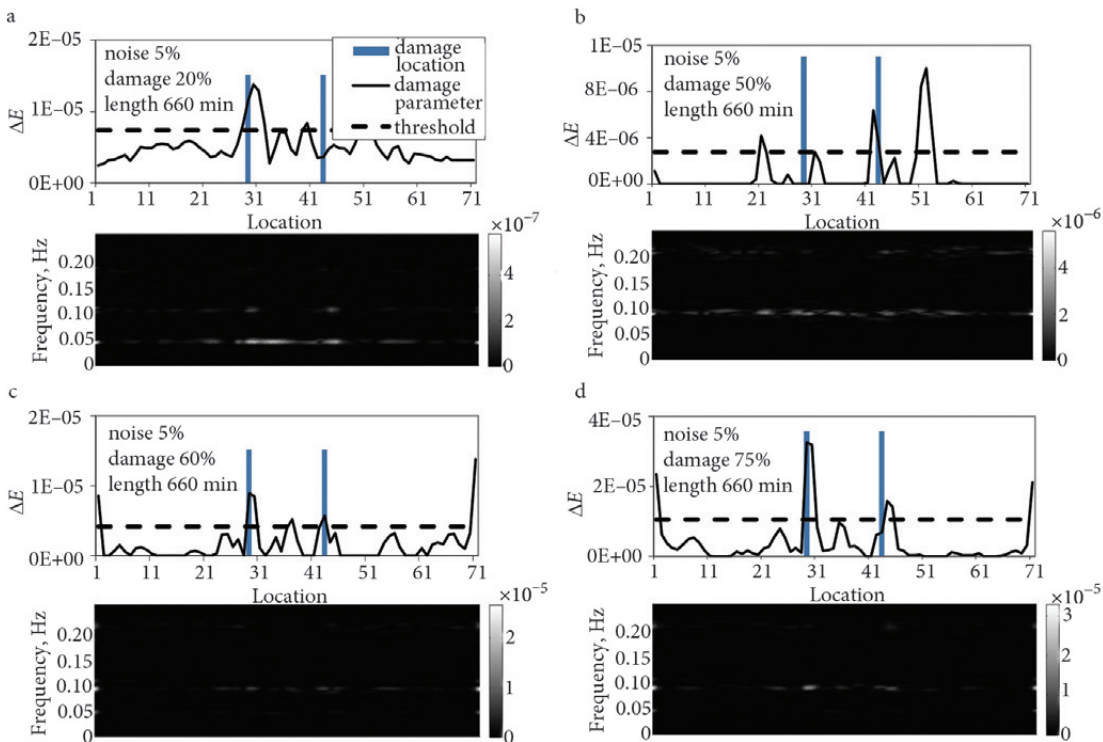


Fig. 9. Multiple damage scenario for response length of 660 min and SNR = 20. Contour bands:  $|E_d(z) - E_o(z)|$

when the noise level increases. This is clearly shown by comparing the figures corresponding to the same noise level and the same record length, but with different damage intensity (e.g. Figs 8a and 8d).

Further increasing the noise, as shown in Fig. 9 which corresponds to 5% noise, even very long signals (660 min) do not allow to correctly locate damage, and false alarms appear for low to high damage severity. Only in the case of a very large stiffness reduction (a stiffness decrement of 75% of the original value), the correct damage locations can be detected (Fig. 9d) although some false alarms can be observed at the structure's boundary (locations N1 and N71). These are due to the simplified boundary conditions of the spline interpolation.

The comparison of Figs 6–9 allows for the following comments. As the damage intensity increases, it increases correspondingly the accuracy of the IDDM in detecting the damage locations, although some false alarms can be observed in Figs 9c and 9d. As it is pointed out by Figs 6 and 7, to the increase of the noise level (Fig. 8) the accuracy and the sensitivity of the procedure decreases, also using longer responses. It must be considered, however, that no filtering that could have enhanced the SNR has been applied to the signals. It is noted that the numerical model was able to simulate the geometrical nonlinearities affecting the response of the long span bridge. Results show that such effects do not alter the effectiveness of the IDDM in detecting damages.

The possibility, successfully investigated in this paper, to apply the IDDM using data from ambient vibrations, together with its simplicity and low computational cost, makes it appealing for being automated and implemented for permanent structural health monitoring applications.

## 7. Conclusions

The sensitivity to noise of the Interpolation Damage Detection Method was checked for a suspension bridge based on responses to the wind-induced vibrations of a calibrated finite element model. Effect of noise was evaluated for different damage intensities and positions with respect to a number of damage scenarios. Damage is modeled by a reduction, at several different positions, of the local stiffness in bridge deck members. Both noise-free and noise-polluted scenarios were considered in the numerical simulation.

1. In this paper the Interpolation Damage Detection Method has been demonstrated effective at the numerical level for the Level II damage identification (damage localization) on a wind excited long-span bridge.

2. Results show that the Interpolation Damage Detection Method gives reliable results also in cases where geometric nonlinearities can influence the structural response.

3. Noise causes random variations of the damage parameter, affecting the method sensitivity. As a remedial measure, if low-noise sensors cannot be deployed, an increase of length of the recorded signals is a feasible way to mitigate the noise negative effects and increase the sensitivity of the damage detection method. This was clearly

shown by the comparison between scenarios relating to the same level of damage and noise, but different records length.

Should long recoding be not feasible, a substitute solution, as response filtering, has to be sought to decrease the noise effects.

## Acknowledgments

This work has been partially supported by the ReLuis-DPC Executive Project 2014–2016, Special Project “Monitoring”, whose contribution is gratefully acknowledged. Mr. Masahiro Nishitani (Honshu-Shikoku Bridge Expressway JP) providing original data and measures on the structure is gratefully acknowledged.

## References

- Abdel-Ghaffar, A. M.; Scanlan, R. H. 1985. Ambient Vibration Studies of Goldengate Bridge I: Suspended Structure, *Journal of Engineering Mechanics ASCE* 111(4): 463–482. [http://dx.doi.org/10.1061/\(ASCE\)0733-9399\(1985\)111:4\(463\)](http://dx.doi.org/10.1061/(ASCE)0733-9399(1985)111:4(463))
- Allemang, R. J.; Brown, D. L. 1982. A Correlation Coefficient for Modal Vector Analysis, in *Proc. of the 1<sup>st</sup> International Modal Analysis Conference (IMAC)*, 8–10 November 1982, Orlando, Florida. 110–116.
- Brownjohn, J. M. W.; Dumanoglu, A. A.; Severn R. T.; Taylor, C. A. 1987. Ambient Vibration Measurements of the Humber Suspension Bridge and Comparison with Calculated Characteristics, *Proceedings of the Institution of Civil Engineers* 83(3): 561–600. <http://dx.doi.org/10.1680/iucep.1987.335>
- Casciati, S.; Domaneschi, M.; Inaudi, D. 2005a. Damage Assessment from SOFO Dynamic Measurements, in *Proc. of SPIE – The International Society for Optical Engineering* 5855: 1048–1051. <http://dx.doi.org/10.1117/12.623656>
- Casciati, S.; Domaneschi, M.; Inaudi, D. 2005b. Local Damage Detection from Dynamic SOFO Experimental Data, in *Proc. of SPIE – The International Society for Optical Engineering* 5765: 591–599. <http://dx.doi.org/10.1117/12.600440>
- Catbas, F. N.; Aktan, A. E. 1999. Vibration Testing of a Long Span Bridge: Objectives and Challenges, in *Proc. of IMAC XVII - 17<sup>th</sup> International Modal Analysis Conference*, 8–11 February 1999, Orlando, US. 166–173.
- Cunha, A.; Caetano, E.; Magalhães, F.; Moutinho, C. 2013. Recent Perspectives in Dynamic Testing and Monitoring of Bridges, *Structural Control and Health Monitoring* 20(6): 853–877. <http://dx.doi.org/10.1002/stc.1516>
- Dilena, M.; Limongelli, M. P.; Morassi A. 2014. Damage Localization in Bridges via FRF Interpolation Method, *Mechanical Systems and Signal Processing* 52–53: 162–180. <http://dx.doi.org/10.1016/j.ymssp.2014.08.014>
- Doebbling, S. W.; Farrar, C. R.; Prime, M. B. 1998. A summary Review of Vibration-Based Damage Identification Methods, *The Shock and Vibration Digest* 30: 91–105. <http://dx.doi.org/10.1177/058310249803000201>
- Domaneschi, M.; Martinelli, L. 2014. Refined Optimal Passive Control of Buffeting-Induced Wind Loading of a Suspension Bridge, *Wind and Structures* 18(1): 1–20. <http://dx.doi.org/10.12989/was.2014.18.1.001>

- Domaneschi, M.; Martinelli, L. 2013. Optimal Passive and Semi-active Control of a Wind Excited Suspension Bridge, *Structure and Infrastructure Engineering* 9(3): 242–259. <http://dx.doi.org/10.1080/15732479.2010.542467>
- Domaneschi, M.; Limongelli, M. P.; Martinelli, L. 2013a. Vibration Based Damage Localization Using MEMS on a Suspension Bridge Model, *Smart Structures and Systems* 12(6): 679–694. <http://dx.doi.org/10.12989/sss.2013.12.6.679>
- Domaneschi, M.; Limongelli, M. P.; Martinelli, L. 2013b. Multi-Site Damage Localization in a Suspension Bridge via After-shock Monitoring, *International Journal of Earthquake Engineering* 30(3): 56–72
- Domaneschi, M.; Limongelli, M. P.; Martinelli, L. 2013c. Interpolation Damage Detection Method on a Suspension Bridge Model: Influence of Sensors Disturbances, *Key Engineering Materials* 569–570: 734–741. <http://dx.doi.org/10.4028/www.scientific.net/KEM.569-570.734>
- Domaneschi, M.; Limongelli, M. P.; Martinelli, L. 2012. Damage Detection in a Suspended Bridge Model Using the Interpolation Damage Detection Method, in *Proc. of the 6<sup>th</sup> International Conference on Bridge Maintenance, Safety and Management (IABMAS 2012)*, 8–12 July 2012, Stresa (VB), Italy. 2975–2980.
- Hao, H.; Oliveira, C. S.; Penzien, J. 1989. Multiple-Station Ground Motion Processing and Simulation Based on SMART-1 Array Data, *Nuclear Engineering and Design* 111(3): 293–310. [http://dx.doi.org/10.1016/0029-5493\(89\)90241-0](http://dx.doi.org/10.1016/0029-5493(89)90241-0)
- He, X.; Moaveni, B.; Conte, J. P.; Elgamal, A.; Masri, S. F. 2008. Modal Identification Study of Vincent Thomas Bridge Using Simulated Wind-Induced Ambient Vibration Data, *Computer-Aided Civil and Infrastructure Engineering* 23(5): 373–388. <http://dx.doi.org/10.1111/j.1467-8667.2008.00544.x>
- Hendy, C. R.; Chakrabarti, S. 2014. Fatigue Management of the Midland Links, UK Steel Box Girder Decks, *Proceedings of the Institution of Civil Engineers: Bridge Engineering* 167(2): 143–154. <http://dx.doi.org/10.1680/bren.11.00007>
- Hester, D.; González, A. 2015. A Bridge-Monitoring Tool Based on Bridge and Vehicle Accelerations, *Structure and Infrastructure Engineering: Maintenance, Management, Life-Cycle Design and Performance* 11(5): 619–637. <http://dx.doi.org/10.1080/15732479.2014.890631>
- Limongelli, M. P. 2011. The Interpolation Damage Detection Method for Frames under Seismic Excitation, *Journal of Sound and Vibration* 330(22): 5474–5489. <http://dx.doi.org/10.1016/j.jsv.2011.06.012>
- Limongelli, M. P. 2010. Frequency Response Function Interpolation for Damage Detection under Changing Environment, *Mechanical Systems and Signal Processing* 24(8): 2898–2913. <http://dx.doi.org/10.1016/j.ymssp.2010.03.004>
- Mohd-Yasin, F.; Nagel, D. J.; Korman, C. E. 2010. Noise in MEMS, *Measurement Science and Technology* 21(1): 1–22. <http://dx.doi.org/10.1088/0957-0233/21/1/012001>
- Nguyen, K. V.; Tran, H. T. 2010. Multi-Cracks Detection of a Beam Like Structure Based on the on-Vehicle Vibration Signal and Wavelet Analysis, *Journal of Sound and Vibration* 329(21): 4455–4465. <http://dx.doi.org/10.1016/j.jsv.2010.05.005>
- Ratcliffe, C. P. 2000. A Frequency and Curvature Based Experimental Method for Locating Damage in Structures, *Transactions of the American Society of Mechanical Engineers Journal of Vibration and Acoustics* 122(3): 324–329. <http://dx.doi.org/10.1115/1.1303121>
- Sampaio, R. P. C.; Maia, N. M. M.; Silva, J. M. M. 1999. Damage Detection Using the Frequency Response Function Curvature Method, *Journal of Sound and Vibration* 226(5): 1029–1042. <http://dx.doi.org/10.1006/jsvi.1999.2340>
- Solari, G.; Piccardo, G. 2001. Probabilistic 3-D Turbulence Modeling for Gust Buffeting of Structures, *Probabilistic Engineering Mechanics* 16(1): 73–86. [http://dx.doi.org/10.1016/S0266-8920\(00\)00010-2](http://dx.doi.org/10.1016/S0266-8920(00)00010-2)
- Soong, T. T. 2004. *Fundamentals of Probability and Statistic for Engineers*. John Wiley & Sons, Inc. 408 p.
- Zhu, X. Q.; Law, S. S. 2006. Wavelet-Based Crack Identification of Bridge Beam from Operational Deflection Time History, *International Journal of Solids and Structures* 43(7–8): 2299–2317. <http://dx.doi.org/10.1016/j.ijsolstr.2005.07.024>
- Zhou, Z.; Wegner, L. D.; Sparling, B. F. 2007. Vibration-Based Detection of Small-Scale Damage on a Bridge Deck, *Journal of Structural Engineering* 133(9): 1257–1267. [http://dx.doi.org/10.1061/\(ASCE\)0733-9445\(2007\)133:9\(1257\)](http://dx.doi.org/10.1061/(ASCE)0733-9445(2007)133:9(1257))

Received 11 August 2013; accepted 5 February 2015